# **CHAPTER 39**

# Modeling the Transformation of Nonlinear Waves Passing over a Submerged Dike

Takumi Ohyama<sup>1</sup> and Kazuo Nadaoka<sup>2</sup>

## <u>Abstract</u>

The decomposition phenomenon of a nonlinear wave train passing over a submerged dike has been investigated by a previously developed numerical model. The model, based on the time-dependent boundary element method, employs an effective nonreflective open boundary treatment and can be applied to arbitrary nonlinear wave processes. The results for regular wave incidence indicate that the higher harmonics generated during passage over the dike are transformed into prominent free waves in the trailing side of the dike, revealing the essential mechanism of the observed decomposition phenomenon. The computed wave profiles at various locations agree favorably with experimental observations. The transformation of multicomponent random waves has also been investigated. The results show that a substantial amount of wave energy is transferred into higher frequency components. The power spectrum of the transmitted wave is found to be significantly influenced by the phase differences among the incident components as well as by the incident wave spectrum itself.

#### 1. Introduction

The decomposition phenomenon of waves passing over a submerged dike is directly related to the variation of wave spectrum and therefore of great importance for predictions of coastal wave fields and beach profile formation (Hulsbergen, 1974). This phenomenon is believed to be governed by both the nonlinearity and the dispersivity of wave fields.

The methods of numerical approaches to this phenomenon may be classified into the following groups. The first approach is based on shallow-water wave

<sup>&</sup>lt;sup>1</sup>Institute of Technology, Shimizu Corporation, Etchujima 3-4-17, Koto-ku, Tokyo 135, JAPAN

<sup>&</sup>lt;sup>2</sup>Department of Civil Engineering, Tokyo Institute of Technology, O-okayama, Meguro-ku, Tokyo 152, JAPAN

theories, such as Boussinesq's theory. However, because this approach relies on assumptions of both weak nonlinearity and weak dispersivity of wave fields it may not be valid especially for prediction in the trailing side of the dike, where higher harmonics may arise as deep-water waves. In fact, its applications have been restricted to the case of solitary wave evolution (Seabra-Santos et al., 1987). The incidence of periodic wave trains is taken into account in the second approach, which is based on the second-order Stokes' wave theory (Massel, 1984). However, because of the limitation of this wave theory, its application is restricted to the case of a deeply submerged dike in a weakly nonlinear wave field. Thus, the applications of these two approaches have been limited with respect to incident wave conditions and the submergence of the dike. In addition, these approaches cannot directly treat the evolution of random waves composed of multiple-frequency components.

By contrast, the time-dependent boundary element method may apply to a wave field of more general conditions, including an arbitrary nonlinear wave field, since the free-surface boundary condition can be fully incorporated without approximations. The lack of efficient open boundary treatments, however, has made it impossible to deal with the incidence of continuous wave trains and, therefore, in many cases solitary waves have been imposed instead (Cooker et al., 1990). Recently, the authors (Ohyama and Nadaoka, 1991) have successfully developed an idealized "numerical wave tank" model based on the boundary element method. This numerical model employs an effective nonreflective open boundary treatment so that it can be applied to arbitrary wave fields including nonlinear random waves. The present study investigates the decomposition of periodic and random wave trains passing over a rectangular submerged dike by using the previously developed numerical model.

# 2. Numerical Wave Tank Model

Numerical analyses have been performed by using a two-dimensional numerical wave tank model previously developed by the authors (Ohyama and Nadaoka, 1991). At both ends of the computational domain, numerical wave-absorption filters are installed as shown in Fig. 1. The filter is composed of a sponge layer to absorb the incoming shorter waves energy by frictional damping and a Sommerfeld-type radiation boundary at the lee side of the layer to transmit the outgoing longer waves. This numerical wave tank model additionally incorporates a nonreflective wave generator which combines a vertically distributed wave-making source  $(S_S)$ , introduced by Brorsen and Larsen (1987).

A decay term proportional to the velocity magnitude is added to the equation of motion in the sponge layers. Based on the potential theory, the dynamic

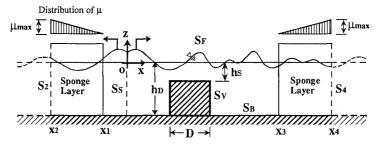


Figure 1. Numerical wave tank model used for the analyses.

condition on the free surface is consequently derived as

$$\frac{\partial \phi}{\partial t} + \frac{1}{2} (\nabla \phi)^2 + g\eta + \mu \phi - \int_{x_1}^x \frac{\partial \mu}{\partial x} \phi \Big|_{on \ S_F} dx = 0 \quad (on \ S_F), \tag{1}$$

in which  $\phi(x, z, t)$  is the velocity potential,  $\eta$  is the surface elevation from the mean water level, and  $\mu$  is the damping factor. The factor,  $\mu$ , is distributed linearly in the layers as shown in Fig. 1 in order to relieve the wave reflection at the leading side of the layers. Based on the results of the earlier study (Ohyama and Nadaoka, 1991), the maximum value of the damping factor in the sponge layers,  $\mu_{max}$ , is given as  $\mu_{max}\sqrt{h_D/g} = 0.25$  in the subsequent computations.

Since the governing equation for the velocity potential in the fluid domain  $\Omega$  is expressed by a Poisson equation, an integral equation is introduced by applying the second form of Green's theorem. All the boundary conditions except the dynamic condition on  $S_F$ , Eq. (1), are substituted into the integral equation. Another integral equation is derived by applying the method of weighted residuals to Eq. (1). These equations, which involve  $\phi$  (on  $S_F$ ,  $S_V$ ,  $S_2$  and  $S_4$ ) and  $\partial \phi / \partial t$ ,  $\eta$  and  $\partial \eta / \partial t$  (on  $S_F$ ) as unknown variables, are discretized spatially and solved simultaneously for successive time steps.

The nodal points on the free surface,  $S_F$ , are considered to move in a vertical direction with the time step advance. The unknown variables,  $\phi$ ,  $\partial \phi / \partial t$ ,  $\eta$  and  $\partial \eta / \partial t$ , can be rewritten by using  $\Delta \phi$  and  $\Delta \eta$ , which are the increments of  $\phi$  and  $\eta$ , respectively, during the time increment  $\Delta t$ . In this time-stepping procedure, nonlinear terms, which correspond to the spatial displacement of the nodal point on  $S_F$ , are taken into account for better accuracy (Ohyama, 1990). The linear algebraic equations to be solved for  $\Delta \phi$  (on  $S_F$ ,  $S_V$ ,  $S_2$  and  $S_4$ ) and  $\Delta \eta$  (on  $S_F$ ) are consequently obtained. The earlier paper (Ohyama and Nadaoka, 1991) provides a detailed description of the numerical procedure.

In the subsequent computations, the time increment,  $\Delta t$ , and the horizontal projection of distance between the surface nodes,  $\Delta x$ , are given to be 1/32 of

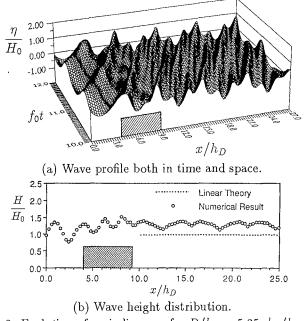
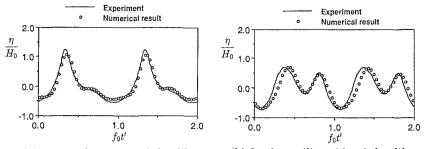


Figure 2. Evolution of periodic wave for  $D/h_D = 5.25$ ,  $h_S/h_D = 0.4$ ,  $\sigma^2 h_D/g = 0.8$ ,  $H_0/h_D = 0.1$ .

incident wave period (or of significant wave period for the case of random waves) and 1/40 to 1/20 of incident wave length (or of significant wave length for the case of random waves), respectively. The initial condition for each case is the still-water condition, i.e.,  $\phi = \eta = 0$ , and numerical results 10 periods after the "cold" start are used for discussion.

## 3. Decomposition Phenomenon of Periodic Waves

Figure 2(a) shows a numerical example of the wave profile around the dike both in time and space, in which  $\sigma$  and  $H_0$  represent the angular frequency and the height of the incident waves. The conspicuous decomposition into the shorter waves occurs immediately after passage over the submerged dike, and the transmitted waves propagate as nonconservative waves composed of multiplefrequency components. The corresponding wave height distribution is indicated in Fig. 2(b), together with the linear solution for transmitted wave height (Ijima and Sasaki, 1971). Preliminary studies found that the linear theory accurately



(a) Above the center of the dike. (b) In the trailing side of the dike. Figure 3. Comparison of computed wave profiles with experimental observations for  $\sigma^2 h_D/g = 0.97$ ,  $h_S/h_D = 0.3$ ,  $H_0/h_D = 0.1$ ,  $D/h_D = 4.0$ .

predicted reflected and transmitted wave energies, even when a conspicuous decomposition of wave trains occurs. As shown in Fig. 2(b), however, the predicted wave height in the trailing side of the dike is markedly greater than the corresponding linear solution, and varies in space since the transmitted waves propagate as nonconservative waves.

The wave evolution during passage through the dike, therefore, produces significant phenomena such as the transfer of a large amount of energy to higher frequency components along with the augmentation of wave height.

### 4. Experimental Verification

Physical model experiments have been conducted to verify the present numerical method. The experimental wave tank is 17m long and 0.4m wide; the water depth,  $h_D$ , and the incident wave height,  $H_0$ , were set at 25cm and 2.5cm, respectively ( $H_0/h_D = 0.1$ ). The model of the submerged rectangular dike has a width of 100cm ( $D/h_D = 4.0$ ) and a height of 17.5cm ( $h_S/h_D = 0.3$ ). The wave profiles were measured at three locations: one over the center of the dike, and the others 125cm apart from the center of the dike on both sides.

Comparisons of wave profiles at a point over the center of the dike and at a point in the trailing side are given in Figs. 3(a) and 3(b), respectively, in which  $f_0$  represents the incident wave frequency  $(= \sigma/2\pi)$ . The computed wave profiles are found to agree favorably with the corresponding experimental observations, indicating the reliability of the present numerical model.

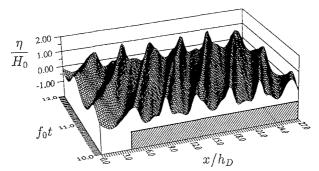


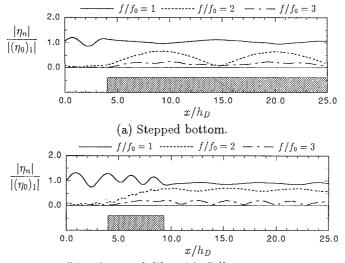
Figure 4. Wave profile both in time and space around stepped bottom for  $h_S/h_D = 0.4$ ,  $\sigma^2 h_D/g = 0.8$ ,  $H_0/h_D = 0.1$ .

#### 5. Mechanism of the Decomposition Phenomenon

Figure 4 shows the computed wave profile for the case of a stepped bottom with  $h_S/h_D = 0.4$ . The incident wave conditions are identical to those of the previous case of the submerged dike (Fig. 2[a]). Figure 4 illustrates that a secondary wave appears at the trailing side of the primary wave as the wave crest propagates onto the step. It then gradually parts from the main crest and is overtaken by the following wave. These basic features of the wave deformation are similar to those of solitary wave disintegration over a stepped bottom (Madsen and Mei, 1969). As indicated in Fig. 2(a), by contrast, wave decomposition during passage over the dike occurs drastically, suggesting that its mechanism is quite different from that of the solitary-wave disintegration over the stepped bottom. Therefore, the wave field in the trailing side of the dike is compared with that over the stepped bottom in order to investigate the mechanism of wave decomposition.

The spatial evolutions of the lowest three harmonic amplitudes,  $|\eta_n|$  (n = 1, 2, 3), are indicated in Figs. 5(a) and 5(b), in which  $|(\eta_0)_1|$  is the first harmonic amplitude of the incident wave. As shown in these figures, the second harmonic amplitude,  $|\eta_2|$ , is spatially modulated over the step, but is preserved in the trailing side of the dike. This modulation phenomenon over the step is explained by *nonlinear resonant interaction* based on the phase mismatch between the free and bound waves in the second harmonic (Mei and Ünlüata, 1972; Bryant, 1973).

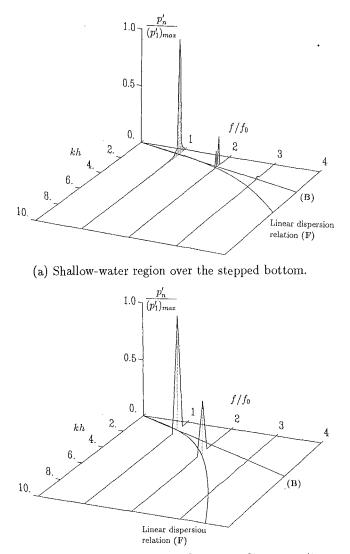
Furthermore, in order to investigate the characteristics of the wave number (or celerity), spectral analyses in the wave number/frequency space have been performed for both the wave field over the stepped bottom  $(6.0 \le x/h_D \le 25.0)$  and that in the trailing side of the dike  $(12.5 \le x/h_D \le 25.0)$ . The results are



(b) Submerged dike with  $D/h_D = 5.25$ . Figure 5. Distribution of each harmonic amplitude for  $h_S/h_D = 0.4$ ,  $\sigma^2 h_D/g = 0.8$ ,  $H_0/h_D = 0.1$ .

indicated in Figs. 6(a) and 6(b), respectively, in which k is the wave number and h is the water depth  $(h = h_S \text{ for the stepped bottom and } h = h_D \text{ for the}$ submerged dike). In the ordinates, the power spectrum for each component,  $p'_n$ , is divided by the maximum value of the spectrum in the first harmonic  $(p'_1)_{max}$ . In each  $f/f_0 - kh$  plain, a curved line (F) represents the linear dispersion relation  $(k \tanh kh = 4\pi^2 f^2/g)$ , and a straight line (B) is drawn from the origin of direction to a point at which the spectrum for the first harmonic  $(f/f_0 = 1)$  is at a maximum. The wave components on line  $(\mathbf{F})$  and those on line  $(\mathbf{B})$  correspond to the free waves and the bound waves, respectively. A larger difference in the celerity between the free and bound waves is found in the trailing side of the dike compared to the case of the stepped bottom. A comparison of the wave number spectra in the second harmonic is indicated in Fig. 7. In the shallowwater region over the stepped bottom, the amount of energy in the bound wave component is larger than that in the free wave component; whereas in the case of the submerged dike almost all the energy of the second harmonic exists as the free wave component.

The results of the spectral analyses yield the following description on the decomposition phenomenon: In the shallow-water region, both the free and bound waves in the higher harmonics result from wave nonlinearity. However, wave



(b) Deep-water region in the trailing side of the dike with  $D/h_D = 5.25$ . Figure 6. Comparison of wave number-frequency spectrum for  $h_S/h_D = 0.4$ ,  $H_0/h_D = 0.1$ ,  $\sigma^2 h_D/g = 0.8$ .

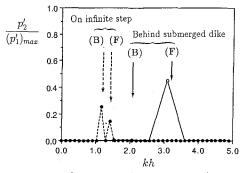


Figure 7. Comparison of wave number spectrum in second harmonic for  $h_S/h_D = 0.4$ ,  $H_0/h_D = 0.1$ ,  $\sigma^2 h_D/g = 0.8$ .

disintegration in this region emerges rather gradually because of the small difference between the celerities of the free and bound waves. When these waves propagate into the deep-water region where wave nonlinearity is so weak that the bound waves can no longer exist, a large amount of energy is transferred abruptly to the free waves in the higher harmonics. Since the celerities are significantly different among the primary wave and these free waves in the deepwater region, the wave disintegration phenomenon is conspicuous compared to the case of the stepped bottom.

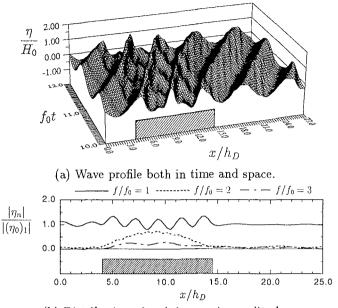
#### 6. Variation in Decomposition Phenomenon According to Dike Width

As shown in Fig. 5(a), the second harmonic amplitude fluctuates spatially over the shallow-water region. Assuming the weak nonlinearity of a wave field, the beat length of  $|\eta_2|$ ,  $\lambda_2$ , can be expressed in the following form (Massel, 1983):

$$\lambda_2 = 2\pi/(k_2 - 2k_1), \tag{2}$$

where  $k_1$  and  $k_2$  represent the wave numbers of the free waves in the first and second harmonics, respectively. The beat length of  $|\eta_2|$  in Fig. 5(a) agrees favorably with the value calculated from Eq. (2).

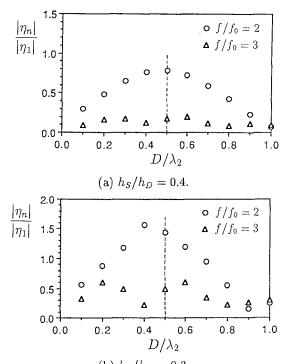
According to the aforementioned mechanism of wave decomposition, it is expected that the amount of energy transferred into the free wave components varies appreciably with the dike width, and that the dike width relative to the beat length of  $|\eta_n|$ ,  $D/\lambda_n$ , is a definitive parameter, as suggested by Mei and Ünlüata (1972). The first numerical example indicated in Figs. 2(a) and 2(b) corresponds to the case of  $D/\lambda_2 = 0.5$  ( $\lambda_2/h_D = 10.5$ ), while Figs. 8(a) and 8(b) show the numerical results for  $D/\lambda_2 = 1.0$ , in which the dike width is twice as



(b) Distribution of each harmonic amplitude. Figure 8. Wave deformation around submerged dike for  $D/h_D = 10.5$ ,  $h_S/h_D = 0.4$ ,  $\sigma^2 h_D/g = 0.8$ ,  $H_0/h_D = 0.1$ .

large as in the first example. In this case of  $D/\lambda_2 = 1.0$ , the transmitted wave profile is almost sinusoidal and a negligible amount of energy is transferred to the higher frequency components during passage over the dike, although nonlinear effects such as steepened wave crests can be seen over the dike. Comparison of Fig. 8(b) with Fig. 5(a) reveals that the distribution of  $|\eta_2|$  over the dike is similar to that over the corresponding stepped bottom.

The variations in  $|\eta_2|$  and  $|\eta_3|$  of the transmitted waves, with  $D/\lambda_2$ , are indicated in Figs. 9(a) and 9(b) for the cases of  $h_S/h_D = 0.4$  and 0.3, respectively. In the ordinates, the higher harmonic amplitudes are normalized with the first harmonic amplitude. Since  $|\eta_2|$  and  $|\eta_3|$  are slightly modulated even in the trailing side of the dike, spatially averaged values over each beat length are plotted in these figures. The results for  $h_S/h_D = 0.4$  (Fig. 9[a]) show that the maximum value of  $|\eta_2|$  appears at  $D/\lambda_2 = 0.5$  and the minimum value at  $D/\lambda_2 = 1.0$ , substantiating that the modulation of  $|\eta_2|$  over the dike is similar to that over the stepped bottom and its value at the trailing edge is preserved in the transmitted wave. In the case of  $h_S/h_D = 0.3$  (Fig. 9[b]), on the other



(b)  $h_S/h_D = 0.3$ . Figure 9. Variation in  $|\eta_n|$  of transmitted waves with  $D/\lambda_2$  for  $\sigma^2 h_D/g = 0.8$ ,  $H_0/h_D = 0.1$ .

hand, the value of  $D/\lambda_2$ , where  $|\eta_2|$  attains its maximum, is smaller than 0.5. This may be because the wave nonlinearity over the dike is so strong that the use of  $\lambda_2$  obtained from Eq. (2) is no longer adequate. Furthermore, in this condition, since the beat length of  $|\eta_3|$  over the step is nearly one-half of  $\lambda_2$ ,  $|\eta_3|$ becomes the minimum at the location where  $|\eta_2|$  is at the maximum, and the peaks of  $|\eta_3|$  appear on both sides.

These results lead to the following conclusions: As inferred by Mei and Ünlüata (1972), each harmonic amplitude in the transmitted waves becomes remarkably larger when  $D/\lambda_n$  is nearly 0.5. When the water depth over the dike is very shallow, however, the stronger nonlinearity yields a shorter beat length of  $|\eta_2|$  than predicted from the weakly nonlinear solution.

#### 7. Spectral Transformation of Random Waves

Lastly, this study investigates spectral transformation of random wave trains. The nonlinearity of the incident random waves considered here is so weak that they are expressed as a sum of multiple-frequency components:

$$\eta_{in} = \sum_{n} a_n \sin(k_n x - 2\pi f_n t + \varepsilon_n), \qquad (3)$$

in which  $\eta_{in}$  is the surface elevation of the incident wave train, and  $a_n$ ,  $k_n$ ,  $f_n$  and  $\varepsilon_n$  represent the amplitude, the wave number, the frequency and the phase lag of each component, respectively.

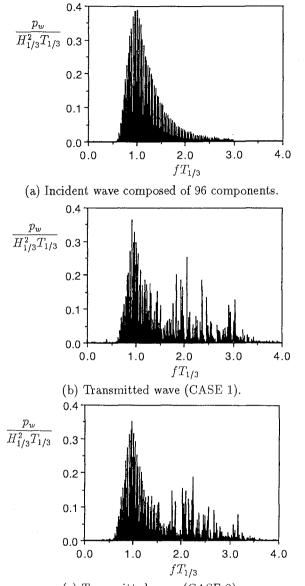
Figures 10(a) - 10(c) show the power spectrum of simulated random incident waves (10[a]), and their modifications through the transmission over a submerged dike with  $D/h_D = 4.0$  and  $h_S/h_D = 0.3$  (10[b] and 10[c]). The incident wave train considered here is composed of 96 wave components and the amplitudes of each component have been prescribed according to the spectrum of Bretschneider-Mitsuyasu (Mitsuyasu, 1970) with  $T_{1/3}\sqrt{g/h_D} = 8.0$ ,  $H_{1/3}/h_D = 0.07$ , in which  $T_{1/3}$  and  $H_{1/3}$  are the significant wave period and height, respectively. The power spectra of the water surface fluctuation were calculated from 4096 wave data at a point  $7h_D$  away from the center of the dike. The power spectrum of the incident waves was obtained from the computation for a flat-bed condition in which the dike does not exist.

In the transmitted wave spectra, several noticeable peaks arise in higher frequency components, indicating that a substantial amount of wave energy is transferred into the higher frequency components. This is of great importance because the augmentation of the wave energy for high frequency makes the significant wave period appreciably shorter. In addition, these spectral peaks are not located as the higher harmonics of the peak frequency of the incident wave spectrum.

Figures 10(b) and 10(c) show the transmitted wave spectra for the incident waves with the same power spectrum (Fig. 10[a]), but with a different series of pseudo-random numbers for the specification of the phase lags among the wave components. The significant difference in the peak frequencies of the wave spectrum between these two cases indicates the importance of the phase difference among the wave components for the transformation of the random wave train.

### 8. Conclusions

The previously developed numerical model has been applied to the analyses of wave decomposition during passage over a submerged dike. The computed wave profiles at various locations agree favorably with experimental observations.



(c) Transmitted wave (CASE 2). Figure 10. Power spectra of random waves for  $T_{1/3}\sqrt{g/h_D} = 8.0$ ,  $H_{1/3}/h_D = 0.07$ ,  $D/h_D = 4.0$ ,  $h_S/h_D = 0.3$ .

The higher harmonics generated over the dike are found to be transformed into prominent free waves in the trailing side of the dike, demonstrating the essential mechanism of the observed decomposition phenomenon. Further computations show that the occurrence of decomposition and its degree depend significantly on dike width. The results for random waves indicate that a substantial amount of wave energy is transferred into higher frequency components. Furthermore, the power spectrum of the transmitted wave is significantly influenced by the phase spectrum of the incident random waves.

# **<u>References</u>**

- Brorsen, M. and J. Larsen. (1987). "Source generation of nonlinear gravity waves with the boundary integral equation method." *Coastal Eng.*, 11, 93-113.
- Bryant, P. J. (1973). "Periodic waves in shallow water," J. Fluid Mech., 59, 625-644.
- Cooker, M. J., D. H. Peregrine, and J. W. Dold. (1990). "The interaction between a solitary wave and a submerged semicircular cylinder." J. Fluid Mech., 215, 1-22.
- Hulsbergen, C. H. (1974). "Origin, effect and suppression of secondary waves," Proc. 14th Coastal Eng. Conf., ASCE, Chapt. 22, 392-411.
- Ijima, T. and Sasaki, T. (1971). "Theoretical studies on effects of a submerged breakwater 1. Impermeable breakwater," Proc. 18th Japanese Conf. Coastal Eng., JSCE, 141-147, (in Japanese).
- Madsen, O. S. and Mei, C. C. (1969). "The transformation of a solitary wave over an uneven bottom," J. Fluid Mech., 39, 781-791.
- Massel, S. R. (1983). "Harmonic generation by waves propagating over a submerged step." Coastal Eng., 7, 357-380.
- Mei, C. C. and Ü. Ünlüata. (1972). "Harmonic generation in shallow water waves." Waves on Beaches, edited by R. E. Meyer, Academic, New York, 181-202.
- Mitsuyasu, H. (1970). "Growth of the spectrum of wind-generated waves (2)," Proc. 17th Japanese Conf. Coastal Eng., 1-7, (in Japanese).
- Ohyama, T. (1990). "A numerical method of solitary wave forces acting on a large vertical cylinder," Proc. 22nd Coastal Eng. Conf., ASCE, Chapt. 64., 840-852.
- Ohyama, T. and K. Nadaoka. (1991). "Development of a numerical wave tank for analysis of nonlinear and irregular wave field." Fluid Dyn. Res., 8, 231-251.
- Seabra-Santos, F. J., Renouard, D. P. and Temperville, A. M. (1987). "Numerical and experimental study of the transformation of a solitary wave over a shelf or isolated obstacle," J. Fluid Mech., 176, 117-134.